

Mixed-Reality Validation of Separation Assurance and Vector Field Guidance for Safe and Conformant Airspace Corridor Integration

Rodolphe Fremond^{†*}, Matthieu Verdoucq^{†*}, Pierre Mazurier[†], Murat Bronz^{†‡}

[†]ENAC Airbus Sopra Steria Drones and UTM Research Chair

[‡]Fédération ENAC ISAE-SUPAERO ONERA, Université de Toulouse, Toulouse, France

{rodolphe.fremond, matthieu.verdoucq, pierre.mazurier, murat.bronz}@enac.fr

Abstract—To accommodate increasing demand for Unmanned Aircraft System (UAS) operations, UAS Traffic Management (UTM) systems must evolve to efficiently scale with higher traffic densities. At this stage, such evolution requires validation with real-world data and testing under realistic operational conditions. Current U-Space approaches ensure safety primarily through spatial and temporal allocation of operational volumes for flight plan authorisation; however, future scalability may require more dynamic flow management models.

This paper presents a mixed-reality demonstration, generalisable for dimensionless scaling operations, of a shared airspace corridor where autonomous UAS follow a Guiding Vector Field (GVF), used for both path-following inside the corridor and smooth entry transitions from vertiports. It is complemented by a hybrid safety and centralised architecture that combines Control Barrier Function (CBF) regulating UAS speed for separation assurance, with an Artificial Potential Field (APF) algorithm for reactive collision avoidance. Deployed in a mixed-reality environment across 88 missions, including over 30 real-world flights, our framework successfully managed continuous, efficient and safe operations within a network of 7 vertiports, supporting up to 6 simultaneous operations inside a 20 × 20 metres shared cyclic corridor scenario with reliable path conformance.

Keywords—Advanced Air Mobility, Control Guidance, Mixed-Reality Simulation, Separation Assurance, Unmanned Aircraft System Traffic Management

I. INTRODUCTION

Fleets of Unmanned Aircraft Systems (UAS) and Urban Air Mobility (UAM) operations are expected to proliferate across urban, suburban, and rural environments, addressing a growing demand for diverse applications. While Air Navigation Services (ANS) have long ensured that aviation remains the safest mode of transportation, current ecosystem does not yet accommodate such traffic at Very Low Level (VLL) airspace. The introduction of U-Space in Europe, orchestrated through the provision of UAS/UAM Traffic Management (UTM) services, aims to integrate these operations in harmony with existing ANS standards and operational practices [1]. This transition supports the modernisation of Air Traffic Management (ATM) in addition to respond to critical responsibilities concerning safety and other key considerations when deploying UAS and UAM operations in close proximity to civilian populations [2].

This research is funded by ENAC - Airbus - Sopra Steria, Drones and UTM Research Chair.

*These authors contributed equally to this work.

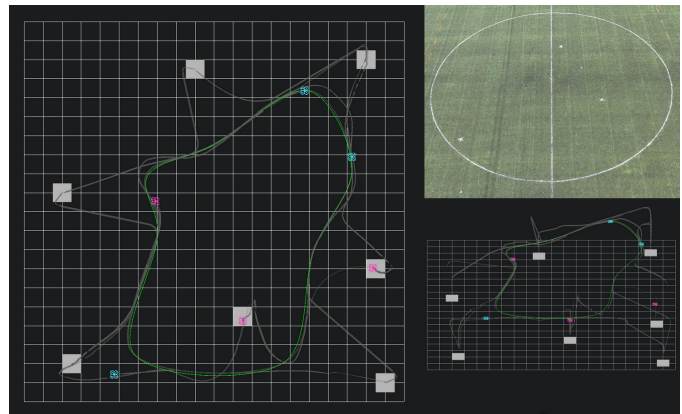


Figure 1. Three-view depiction of the scenario: top-down airspace layout (left), isometric simulation perspective (bottom right), and real-world flight zone (top right). The scenario featured a mixed fleet of 3 simulated and 3 real UAVs operating concurrently.

The SESAR CORUS project, CORUS-XUAM and now CORUS V, has been establishing the foundational operational concepts guiding European U-space research and outlined a phase evolution of services [3]. Building upon this framework, initiatives like the EUREKA project are developing concrete solutions for key challenges, including the integration of vertiports into the airspace management [4]. It aims to define arrival/departure procedures and design airspace structures, considering urban corridors, for Vertical Take-Off Landing (VTOL) capable aircraft [5].

Concurrently, academic research has proposed various concepts for managing traffic in the terminal area around vertiports. For instance, the Vertiport Terminal Area Controller (VTAC) concept utilises a concentric ring-based airspace design and computational guidance for safe transitions [6]. Subsequent work has explored alternatives using Reinforcement Learning with indoor deployments [7], or queue management systems resembling a “spider web” structure [8], [9].

The validation of these concepts requires moving beyond pure simulation. The use of mixed-reality and digital twins is gaining traction for UAM validation, enabling risk-free analysis of complex scenarios. For example, recent work has focused on high-fidelity digital twins for vertiport capacity evaluation [10] and interactive 3D exploration [11].

Despite the industrial push for Digital Twins, academic research on UTM often remains confined to simplified sandbox simulations. These are typically miniaturised, lack operational realism, and fall short to demonstrate end-to-end performance at scale. Mixed-reality approaches are underutilised for their potential to safely explore safety-critical operations where synthetic components can mitigate corporal and material damages while enabling validation against real-world behaviour. There is a critical need for operationally meaningful mixed-reality frameworks that bridge simulation, experimentation, and live deployment to provide the feedback loop currently missing in UTM development.

Current U-Space regulations mandate strategic conflict resolution as a prerequisite for flight authorisation [12]. This framework treats the operational volume as a static block to be reserved, ensuring the highest level of safety during the initial emergence of U-space operations. As traffic density increases to meet on-demand UAS needs, this first-come first-served model may rapidly face scalability limitations [13]. Transitioning towards dynamic operational flows using shared spatial volumes is a promising path to improve the overall efficiency of the airspace at the VLL [14], but strategic separation minima alone are insufficient to guarantee safety in this context. Even coupled with a robust vertiport schedule management, unanticipated trajectory intersections and a loss of separation could occur under competitive traffic patterns or due to real-time perturbations such as weather deviations, delays, or priority vehicle insertions from vertiports.

Our research contrasts to the static reservation model on the investigation of a dynamic flow within a self-organised shared corridor for the U-Space airspace. To bridge the gap, we present a mixed-reality framework and associated methods with the following key contributions:

- Developing and demonstrating a scalable, dimensionally-generalisable mixed-reality simulation environment that integrates real and simulated drones within a unified U-space airspace, supporting the safe validation of safety-critical operations in self-organised corridors under realistic traffic conditions and opening a pathway to full-scale Beyond Visual Line of Sight (BVLOS) deployment.
- Proposing a novel application of the Guiding Vector Field (GVF) for smooth and predictable transitions between vertiports and an airspace corridor, decoupling scheduling logic from tactical guidance to support on-demand operations.
- Proposing a layered separation assurance architecture combining a Control Barrier Function (CBF) for longitudinal speed control and an Artificial Potential Field (APF) algorithm for reactive collision avoidance to maintain safe separation across all flight phases.

This framework is instantiated in a scenario featuring a simple vertiport scheduler for mission management and a cyclic, unidirectional airspace corridor, building upon our previous work to demonstrate its safety [15], [16], and enable continuous operations during the experiments.

The paper is structured as follows: Sec. II details the methodologies, Sec. III presents the experimental setup and

results, Sec. IV discusses these results, and Sec. V concludes the research.

II. METHODS

Sec. II-A introduces the UAV guidance mechanism, and Sec. II-B provides a high-level view of the mixed-reality simulation framework

A. Cooperative Guidance Mechanism

In this research, all vehicles; whether real or simulated, are assumed to be autonomous and share a common unidirectional airspace corridor. To coordinate traffic within the corridor, as well as during transitions between vertiports and the corridor, a GVF is employed, as formulated in Sec.II-A1. The design of entry and exit transitions is presented in Sec.II-A2. Sec. II-A3 details the VTOL process, and Sec. II-A4 provides a summary of the airspace user mission. Finally, Sec.II-A5 introduces the separation assurance functions used to prevent airborne conflicts between operations.

1) *Guiding Vector Field Formulation* : The airspace corridor is modelled as a GVF that attracts nearby operations towards the centreline and provides progression along it once captured [17]. In practice, the corridor \mathcal{C} is represented by a continuous curve interpolating a finite set of waypoints \mathcal{C}_{wpt} .

Let the corridor centreline, of total length \mathcal{C}_{len} and at a fixed flight level \mathcal{C}_z , be a continuously differentiable curve $\gamma : [0, \mathcal{C}_{len}] \rightarrow \mathbb{R}^3$, parameterised by arc length s . Its unit tangent is $\mathcal{T}(s) = \frac{\dot{\gamma}(s)}{\|\dot{\gamma}(s)\|}$. Given an aircraft position $p \in \mathbb{R}^3$, the closest-point projection is $\mathcal{C}(p) = \gamma(s^*(p))$, with $s^*(p) \in \arg \min_{s \in [0, \mathcal{C}_{len}]} \|p - \gamma(s)\|$. The GVF is then defined as $\mathcal{G}(p) = \sigma k_T \mathcal{T}(s^*(p)) + k_N (\mathcal{C}(p) - p)$, where $\sigma \in \{-1, 1\}$ is the direction selector, k_T is the tangential gain providing progression along the corridor, and k_N is the attraction gain pulling the aircraft towards the centreline. Both gains are strictly positive. The resulting unit-norm velocity command is $u_{GVF}(p) = \frac{\mathcal{G}(p)}{\|\mathcal{G}(p)\|}$.

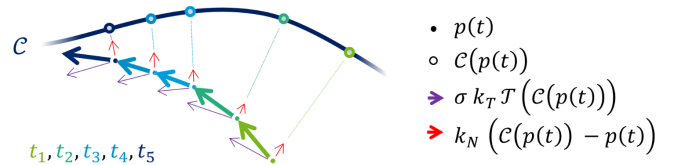


Figure 2. Example of GVF-based transition sequence from a vertiport to a corridor with decomposition of tangential and normal terms.

2) *Corridor Transitions Design* : To enable the integration from vertiports to the corridor, each vertiport v is associated with two transition points defined along the corridor centreline: an entry point $s_C^{(in)}(v)$ and an exit point $s_C^{(out)}(v)$. Let $s_C^*(v)$ denote the curvilinear abscissa of the closest projection of the vertiport position onto the corridor \mathcal{C} . The entry and exit points are then defined by fixed offsets along the flow direction: $s_C^{(in)}(v) = (s_C^*(v) + \Delta s_C^{(in)}) \bmod \mathcal{C}_{len}$, and $s_C^{(out)}(v) = (s_C^*(v) - \Delta s_C^{(out)}) \bmod \mathcal{C}_{len}$, where $\Delta s_C^{(in)} > 0$ and $\Delta s_C^{(out)} > 0$ are configurable offsets. As illustrated in Fig.

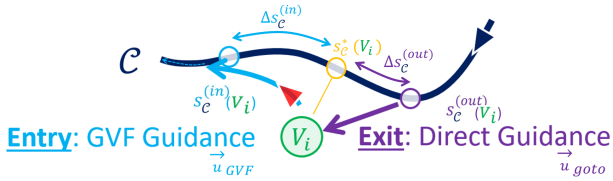


Figure 3. Corridor Transitions: Entry and Exiting.

3, the entry point lies downstream of the vertiport projection and serves as the logical gate through which traffic must be scheduled before merging into the corridor, while the exit point lies upstream and defines where a vehicle must leave the corridor flow before proceeding to its destination vertiport.

It is important to note that these transition points serve primarily as scheduling and triggering references rather than direct control targets. Practically, they act as scheduling hooks, not as waypoints to be chased. During the entry phase, vehicles are guided by the GVF using their closest-point projection onto the corridor rather than by steering directly towards $s_c^{(in)}$. This ensures a stable capture of the centreline without oscillations around a fixed entry gate. A vehicle cruising accurately along the corridor centreline is influenced only by the tangential component of the GVF \mathcal{G} , as the attractive terms are null (i.e., $\mathcal{C}(p) - p \approx 0$). Then, minor deviations are easily corrected to restore the vehicle to the centreline.

Upon reaching $s_c^{(out)}$, the GVF guidance is released and the vehicle executes a direct go-to manoeuvre, instructed by \vec{u}_{goto} , towards its destination vertiport.

3) *Vertical Take-off and Landing* : VTOL phases are designed for simplicity and efficiency, as illustrated in Fig. 1.

During departure from a vertiport v at the Above Ground Level (AGL) altitude Δz_{VTOL} , the UAV climbs vertically to an intermediate altitude $z_C(v)$ at a vertical speed \dot{z} and aligns with a lateral offset $\Delta v_{r_{VTO}}$. This altitude $z_C(v)$ marks the transition from take-off to the corridor entry procedure described in Sec. II-A2. It is calculated to achieve a climb angle of approximately 45 degrees relative to the vertiport, with a minimum value of $\mathcal{C}_z/2$ to ensure a feasible transition even for vertiports located farther from the corridor \mathcal{C} . The specific value thus depends on both the corridor's final altitude \mathcal{C}_z and its horizontal distance from the vertiport.

For landing, the UAV remains at \mathcal{C}_z during the exit phase and aligns with the arrival vertiport with an offset of $\Delta v_{r_{VL}}$ before performing the final descent to the vertiport at the AGL altitude Δz_{VTOL} .

4) *Vertiport Management & Authorisation* : Vertiport management is a wide and complex topic that deserves its own dedicated research. While not the main focus of our work, we assume that airspace users' missions transit through the operational phases depicted in Fig. 4. A straight forward key



Figure 4. Sequence of operational phases for a single mission, from pre-departure to landing.

consideration in this cycle is the management of vertiport slots considering destination vertiports entirely blocked.

During the scheduling period, operations check for available destination slots at vertiports. Once a slot is assigned to an operator, it is blocked and cannot be assigned to any other operator as a destination. The operational life cycle continues with the operator awaiting departure at a vertiport. At this stage, the vertiport occupied by the operator becomes available as a destination for other traffic, and the operator executes a take-off as described in Sec. II-A3. The mission then proceeds through the entry transition into the corridor and the cruising phase, both guided by the GVF, followed by the exit transition under direct guidance, as detailed in Sec. II-A2. The final landing phase at the destination vertiport is also described in Sec. II-A3.

Once landed, we consider two options for the destination vertiport slot. The first option, which is conceptually valid but not implemented in our current model, is that the operator is grounded, making the vertiport slot available for other traffic. The second scenario, which is used in our research, assumes the operator has landed but will start another mission; consequently, the vertiport slot remains blocked until the end of the scheduling period. This second option may reflect specific cases like touch-and-go or rapid delivery operations, but it is mostly adopted here to facilitate the modeling of continuous operations.

5) *Separation Assurance* : The guidance approach introduced earlier may raise safety concerns during corridor entry transitions. To cope with the loss of separation events during these transitions and throughout the operation, our approach ensures that all vehicles maintain well-clear conditions with respect to one another. A loss of separation is defined as a breach of the Loss of Well-Clear (LoWC) threshold ρ_{LoWC} .

Whereas separation assurance is preferably preventive, our framework deliberately chose to reactively initiate it once a LoWC breach occurs. Preventive actions may seem intuitively safer but imposes stringent geometric constraints when using the CBF described later in this section; CBF can cause vehicles to halt abruptly within the traffic stream, thereby disrupting flow if the detection is too large or preventive. In our conflict resolution model, each encounter is processed as a pair consisting of an ownship i and an intruder j , where the ownship is responsible for executing resolution manoeuvres based on the states of both aircraft.

First, we adapt a CBF for corridor-speed regulation [18], complemented by a APF approach based on Boid-inspired repulsion mechanism [19]. In some of our experimental settings, this repulsion mechanism is also employed as the main separation assurance method in place of the CBF. The CBF regulates speed to maintain homogeneous flow along the prescribed spatial trajectory. Algorithm 1 outlines its implementation for separation assurance in the presence of multiple potential conflicts. This algorithm is generalised for broad applicability but includes tuning for specific encounter types. It is also important to note that CBF speed regulation only modifies the norm of the velocity vectors \vec{u}_{GVF} and \vec{u}_{goto}

Algorithm 1 Control Barrier Separation Assurance Function

```

1: Initialisation* :  $\Delta t$  ( $\frac{1}{f}$ ),  $\rho_{LoWC}$ ,  $u_{min}$ ,  $u_{max}$ ,  $a_{max}$ ,  $\epsilon$ , traffic tracking
   information at time  $t$ : position, and velocity vectors  $(\vec{p}_i, \vec{u}_i)(t)$ .
2: for vehicle  $i$  in traffic do
3:    $(\underline{u}_i, \bar{u}_i) = (-\infty, \infty)$ 
4:   for vehicle  $j$  in surrounding traffic, with  $j \neq i$  do
5:      $h = \|\vec{p}_i - \vec{p}_j\|^2 - \rho_{LoWC}^2$ 
6:      $\nabla h = 2(\vec{p}_i - \vec{p}_j)$ 
7:      $Lf_h = -\nabla h^\top \vec{u}_j$ 
8:      $a = \nabla h^\top \frac{\vec{u}_i}{\|\vec{u}_i\|} + \epsilon$ 
9:      $b = -(Lf_h + \alpha h)$ 
10:    if  $a > \epsilon$  then
11:       $\underline{u}_i \leftarrow \max(\underline{u}_i, \frac{b}{a})$ 
12:    else
13:       $\bar{u}_i \leftarrow \min(\bar{u}_i, \frac{b}{a})$ 
14:    end if
15:  end for
16:   $\Delta u_i = \text{clip}\left(\|\vec{u}_i(t)\|, \max(\underline{u}_i, u_{min}), \min(\bar{u}_i, u_{max})\right) - \|\vec{u}_i(t)\|$ 
17:   $\|\vec{u}_i(t + \Delta t)\| = \|\vec{u}_i(t)\| + \text{clip}\left(\frac{\Delta u_i}{\Delta t}, -a_{max}, a_{max}\right)\Delta t$ 
18:   $\vec{u}_i(t + \Delta t) = \frac{\vec{u}_i(t)}{\|\vec{u}_i(t)\|} \|\vec{u}_i(t + \Delta t)\|$ 
19: end for

```

* The definitions of the different notations are detailed later in Table II.

to ensure compliance with the current trajectory. Separation is enforced as a horizontal Euclidean distance. This simplified corridor-relative approach assumes the corridor geometry itself provides inherent safety, with properly separated lanes and no intersecting trajectories. However, this assumption heavily depends on reliable strategic planning and requires drones to maintain close adherence to their nominal paths. A main benefit of CBF is its natural ability to prioritise the downstream UAV. In addition, CBF primarily decelerates the UAV, thereby granting priority to the encounter not subject to CBF.

Second, an APF approach mainly works as a collision avoidance system when CBF is not enough or not allowed as a separation assurance function. Detailed in Algorithm 2, this reactive method serves as a fallback for any flight phase and unexpected scenarios. Unlike the CBF's geometrically constrained separation, the APF strategy employs free-form repulsion to prevent Near Mid-Air Collision (NMAC) where corridor assumptions no longer apply, for close-range encoun-

Algorithm 2 Artificial Potential Field Collision Avoidance

```

1: Initialisation: Similar parametrisation than Algorithm 1.
2: for vehicle  $i$  in traffic do
3:    $\Delta \vec{p} = \vec{0}$ 
4:   for vehicle  $j$  in surrounding traffic, with  $j \neq i$  do
5:      $\delta \vec{p}_{i,j} = \vec{p}_i - \vec{p}_j$ 
6:   end for
7:    $\mathcal{D}_i = \{\delta \vec{p}_{i,j} : \|\delta \vec{p}_{i,j}\| \leq \rho^*\}$ 
8:   sort  $\mathcal{D}_i$  by ascending separations ( $\|\delta \vec{p}_{i,j}\|$ ), up to K
9:   for  $\delta \vec{p}$  in  $\mathcal{D}_i$  do
10:     $\Delta \vec{p} \leftarrow \Delta \vec{p} + \delta \vec{p} \cdot \frac{c_{rep}}{\max(\|\delta \vec{p}\|, 0.1)}$ 
11:  end for
12:   $\vec{u}_{sep} = \Delta \vec{p} \cdot u_C$ 
13:  Saturate  $\vec{u}_{sep}$  to  $\|\vec{u}_{sep}\| \leq u_{max}$ 
14: end for

```

* ρ depends on whether the mechanism is applied to separation assurance or to collision avoidance, taking the values ρ_{LoWC} and ρ_{NMAC} , respectively. The same applies to c_{rep} , which is set to 0.5 or 1.0.

ters requiring immediate collision avoidance.

B. Simulation Framework

Sec. II-B1 introduces the centralised hybrid controller, which is the core component of the mixed-reality environment concisely developed in Sec. II-B2.

1) *Centralised Hybrid Controller* : It unifies real and simulated drones under a single decision-making loop. At each cycle, it retrieves positions, updates vehicle phases, and computes new control commands.

To coordinate guidance and speed control across n drones with heterogeneous mission phases, the controller introduces a modular control allocation framework based on flight status detailed in Table I. Each drone generates candidate inputs from the difference guidance laws introduced until there; both geometric vector field speed instruction \vec{u}_{GVF} embedding \vec{u}_{goto} detailed in Sec. 3 and embedding CBF gain detailed in Algorithm 1, APF collision avoidance speed instruction \vec{u}_{APF} detailed in Algorithm 2, and the vertical speed control \dot{z} detailed in Sec. II-A3.

TABLE I. FLIGHT STATUS-RELATED SPEED CONTROL GUIDANCE

	\vec{u}_{GVF}	\vec{u}_{goto}	\vec{u}_{APF}	\dot{z}
VTOL				✓
Entering	✓		✓	✓
Cruising	✓		✓	✓*
Exiting		✓	✓	✓*

* Corrective vertical guidance applied to ensure corridor adherence at the AGL altitude C_z .

2) *Mixed-Reality Environment* : It combines both simulated and physical drones, and is driven by a Python-based backend that loads the scenario configuration (e.g., corridor geometry and vertiports location). Each agent may correspond either to a real DJI drone connected via the DJI SDK interface [20], or to a software mock drone operating in simulation represented by a noise-free first-order model. The centralised hybrid controller, the core orchestrator detailed in Sec. II-B1, unifies both categories by applying the coordination logic and guidance instructions throughout Sec. II-A.

A 3D visualisation system complements this backend as illustrated in Fig. 1. It is based on a web architecture composed of a FastAPI server that aggregates telemetry from all clients and an interactive Vue.js interface with a 3D rendering engine (TresJS). Communication between clients and the server is realised through ZeroMQ, while WebSockets forward the aggregated data to the browser for real-time visualisation. This frontend allows observers to monitor the state of all drones, the airspace corridor, and vertiport activity in real time.

III. EXPERIMENT

This section introduces the experimental setup in Sec. III-A, followed by a safety analysis of the separation assurance and collision avoidance algorithms in Sec. III-B. The results of the mixed-reality demonstration are then presented in Sec. III-C. Supplementary data, including separation distributions, flight schedules, experiment logs, and demo videos, are available online [21].

A. Setup

This work builds upon several preliminary deployments, starting indoors, culminating in the outdoor demonstration presented here. Earlier trials are referenced in the discussion later in Sec. IV-A for context and comparisons. The core airspace structure; a cyclic corridor, remains fixed across all trials. It was generated using a method from our previous work that designs such corridors based on environment features like vertiport and no-fly zone locations [15], [16]. For this study, the corridor and vertiport placements were fixed, with vertiports positioned both near and far from the corridor periphery to create a varied operational scenario.

The experimental scenario, illustrated in Fig. 1, involved a fleet of 6 UAVs operating in a mixed-reality environment. The fleet comprised an even split of 3 real DJI Mini 3 drones and 3 simulated vehicles. A cyclic, shared airspace corridor with a length of 43.69 metres was designed within a 20×20 metres operational volume at an altitude of 4 metres, connecting 7 vertiports. The scenario supported the continuous touch-and-go operations, with take-offs and landings occurring at an altitude of 0.75 metres to accumulate data and real-flight experience. Missions lasted up to 15 minutes and were conducted under environmental conditions featuring W-NW winds with speeds ranging from 5 to 11 kts, ± 3 kts.

Table II completes these specifications with corridor features and parameterisation used throughout the methodology.

TABLE II. SCENARIO SPECIFICATIONS

Symbol	Description	Value	Unit
f	Simulation update rate	10	Hz
ϵ	Small numerical margin	10^{-6}	#
\mathcal{A}	Airspace size	20×20	m^2
n_v	Number of vertiport	7	#
n_{real}	Number of UAV (real)	3	#
n_{sim}	Number of UAV (simulated)	3	#
σ	Corridor direction (clockwise)	1	#
\mathcal{C}_{len}	Corridor length	43.69	m
\mathcal{C}_z	Corridor AGL altitude	4.0	m
\mathcal{C}_{wpts}	Corridor waypoints discretisation	500	#
$\Delta s_C^{(in)}$	Corridor entry transition offset	1	m
$\Delta s_C^{(out)}$	Corridor exit transition offset	1	m
$\Delta v_{r_{VTO}}$	Take-off vertiport radius offset	0.75	m
$\Delta v_{r_{VL}}$	Landing vertiport radius offset	0.75	m
Δz_{VTO}	Vertiport AGL altitude offset	0.75	m
u_C	Nominal (i.e., cruise) speed	1.0	$m.s^{-1}$
u_{min}	Minimum in-cruise speed	0.05	$m.s^{-1}$
u_{max}	Maximum speed	2.0	$m.s^{-1}$
\dot{z}	Maximum vertical speed	0.5	$m.s^{-1}$
a_{max}	Maximum acceleration	1.5	$m.s^{-2}$
k_N	GVF normal gain	10.5	#
k_T	GVF tangential gain	1.0	#
ρ_{LoWC}	Loss of Well-Clear threshold	2.5	m
ρ_{NMAC}	Near Mid-Air Collision threshold	1.25	m

The performance of the proposed framework is evaluated across three key performance areas: safety, traffic adherence, and operational capacity. While previous research has assessed the routing efficiency of the cyclic corridor concept [15], [16], this study focuses on its real-time operational performance.

Safety is evaluated using two spatial separation thresholds, as temporal separation was not required due to the homogeneous performance of the traffic. A LoWC event is recorded when the separation between two vehicles falls below the threshold ρ_{LoWC} , triggering the separation assurance functions detailed in Table III for the specific encounter flight phases. In a traffic stream of cruising UAVs, the CBF protocol functions by slowing down either a trailing (i.e., upstream) UAV or a new UAV during its entry maneuver. A NMAC event is recorded if the separation breaches the ultimate safety boundary ρ_{NMAC} , indicating a failure of the separation assurance layer. In such cases, the APF algorithm for collision avoidance is activated unconditionally.

TABLE III. SEPARATION ASSURANCE AT LOWC THRESHOLD

Ownship		Surrounding Traffic			
		VTOL	Entering	Exiting	Cruising
Ownship	Entering	CBF	CBF	APF	CBF
	Exiting	CBF	APF	CBF	-
	Cruising	-	-	APF	CBF

Traffic Adherence assesses the conformance of UAVs to their intended paths within the corridor. This is measured by analysing the lateral deviation of each vehicle from the corridor centreline.

Operational capacity and demand is evaluated from two perspectives: First, the airspace demand is measured by the entry rate and the number of simultaneous operations within the corridor, indicating the throughput of the shared airspace structure. Second, vertiport capacity is assessed through vertiport saturation, defined as the percentage of time a vertiport is occupied, and the analysis of operational headways to evaluate scheduling efficiency and potential delays.

B. Separation Assurance & Collision Avoidance Analysis

To ensure the safe deployment of real drone operations, we conducted preliminary offline tests of both our separation-assurance and collision-avoidance functions in a fully simulated environment. The objective was to identify configuration settings that guarantee safety and to assess the respective roles and benefits of each safety layer.

Table IV reports results from 20-minute touch-and-go operations under four conditions: without conflict resolution, with APF only, with CBF only, and with both methods combined. The algorithms are activated when encounters meet the conditions specified in Table III which may inevitably fail to trigger in certain situations when only a single algorithm is active. Compared to the real-world scenario and its given parametrisation in Table III, the nominal speed u_C is doubled here to challenge the algorithms.

The results indicate that CBF and APF repulsion act as complementary safety layers. CBF is only triggered once a LoWC is reached, preventing most NMAC. The remaining cases are primarily mitigated when APF repulsion is also active. Without any conflict resolution, two collisions were observed, while the APF-only case recorded a critical separation of 0.5 m, suggesting a potential crash. By contrast, both

TABLE IV. SAFETY ANALYSIS OF OPERATIONS OVER 20 MINUTES

Repulsion	CBF	Operations ¹	LoWC ²	NMAC ²
✓		323	493.8	150.1
	✓	316	473.0	30.0
✓	✓	318	274.7	12.5
		319	171.4	5.0

¹ Completed cycles from take-off to landing.

² Values in seconds (i.e., duration of the incursion).

CBF alone and the combined CBF–APF configuration ensured safer separations, with the latter preventing 96.7% of NMAC events. The use of these algorithms introduces only a slight operational delay, reducing the number of completed cycles by an average of 1.5% over the 20-minute demonstrations.

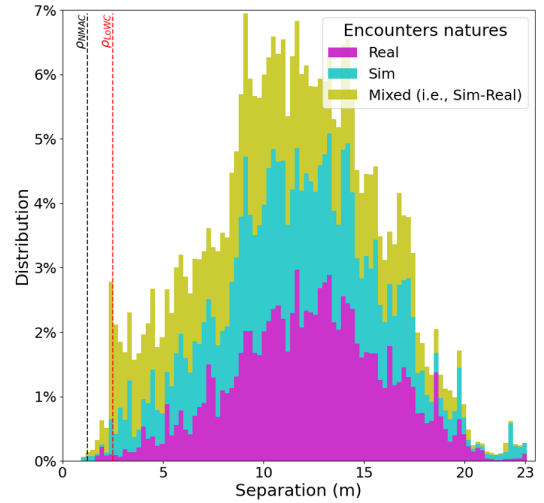
C. Mixed-Reality Scenario Demonstration

The demonstration, conducted with a fleet of six drones, comprised a total of 88 missions (i.e., operational cycles depicted in Fig.4), 33 of which were performed by real UAVs.

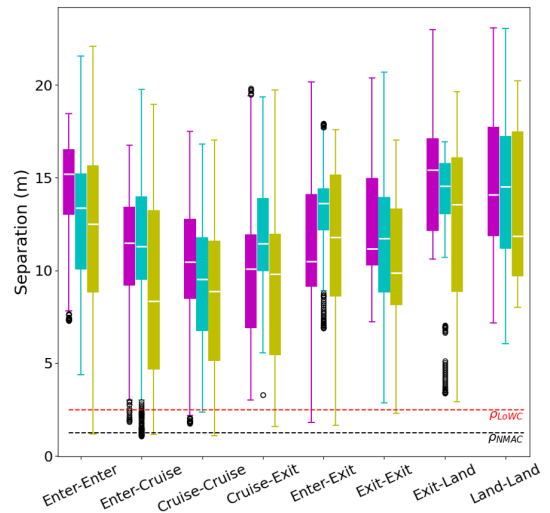
The average vertiport saturation was 38.73%, suggesting that operations are smoothly accommodated under continuous demand. The busiest vertiport was occupied 49.87% of the time, compared to 32.98% for the least occupied. Among occupation events, 1.72% involved a drone approaching an already occupied vertiport, while 10.06% involved simultaneous entry and exit operations. No cases were observed of a drone departing while the vertiport was occupied. The traffic flow corresponded to an average entry rate of 7.95 operations per minute. Within the corridor, the number of simultaneous operations ranged from 0 to 6, with traffic density most often consisting of 2 or 3 concurrent operations. The observed proportions were 10.25%, 15.57%, 24.80%, 24.52%, 16.82%, 6.14%, and 1.90% for 0 through 6 simultaneous mixed operations, respectively.

To address fleet safety management, Fig. 5 presents the distribution of separation between pairs of operations, referred to as encounters. These encounters may involve real UAVs, simulated UAVs, or a mix of both, and are distinguished in the safety evaluation.

First, Fig.5a illustrates the **stacked** distribution of pairwise separations. A large proportion of encounters occur at distances between 10 and 15 metres, which naturally result from the corridor design, extending up to 23 metres for operations on vertiports at opposite sides of the corridor. Below 10 metres, the number of encounters decreases approximately linearly towards the LoWC threshold. A small peak is visible around the LoWC, after which the distribution drops, suggesting that the separation assurance algorithms are effective in repelling encounters to remain just above LoWC. Second, Fig.5b breaks down separations by the flight status of the operations. No NMACs were observed between two real UAVs. However, three NMACs occurred between simulated UAVs and reactively repelled over ρ_{NMAC} , typically when one was entering and the other crossing the corridor, with a cumulative duration of 1.4 seconds. Two additional NMACs involved mixed encounters between real and simulated UAVs



(a) Stacked Separation distribution across encounter types



(b) Separation by flight status of encounters.

Figure 5. Pairwise UAV separation distributions across encounter types and flight statuses, relative to LoWC and NMAC thresholds.

during close entries into the corridor, and one more occurred with both already inside the corridor, totalling 2.2 seconds of NMAC for mixed encounters. LoWC events were also observed between pairs of real UAVs but were appropriately mitigated by the algorithms. The cumulative LoWC durations amounted to 6.0, 10.3, and 128.2 seconds for real, simulated, and mixed encounters, respectively. These durations are cumulative across events and may include simultaneous occurrences from different encounters. Finally, the results show no cases of simultaneous landings or take-offs observed at the same vertiport.

The adherence of the fleet was also studied to assess the difference in trajectory deviations from the corridor between simulated UAVs operating under ideal conditions and real UAVs subject to real-world environmental constraints. Fig.6 shows the trajectories of the real UAVs in magenta colour and those related to simulated UAVs in cyan colour. Real UAVs exhibited systematic deviations near coordinates [-2, -

3.5], reaching up to 0.5 metre likely induced by the corridor geometry. The corridor is appropriately designed for the rest; others deviations are mostly APF repulsion to ensure safe separation according to our observation and suggested by the average deviation in the corridor close to green color, the proximity of the vertiports entry and exiting zones, in addition to similar behaviours of simulated UAVs within the same regions. Under the presented conditions, the deviations of the real UAVs are contained with a corridor width of 1.253 metres with a confidence of 3σ (i.e., 99.73%). High similarities are observed between simulated and real operations during transitions. In particular, real drones closely followed the GVF guidance during entry, while slight but acceptable deviations are noted during corridor exit.

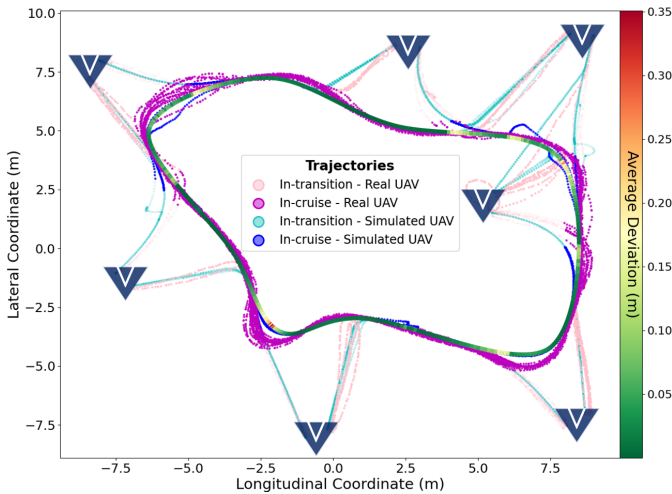


Figure 6. Plotted trajectories of mixed-realism UAV traffic cruising the airspace corridor with representative deviations and transitions. Regions shaded towards the red gradient indicate frequent deviations which may need the need for corridor reshaping, adapted width, or slower operations to maintain conformance. Initial alignments of the real UAVs are not taken into account.

IV. DISCUSSION

This section first interprets the experimental results in Sec. IV-A, then outlines the challenges and limitations encountered in Sec. IV-B, and finally presents directions for future work in Sec. IV-C.

A. Results Analysis

The demonstration presented in Sec. III-C, based on the scenario detailed in Sec. III-A, is discussed here and, where appropriate, qualitatively compared with additional deployments exploring different scales and fleet speeds. The earliest trials were conducted in an 8 x 8 m indoor arena using two Tello drones, without separation assurance algorithms, under a fully controlled environment. These trials served as a stepping stone towards the larger-scale scenario introduced in this paper.

The mixed-reality simulator demonstrated stable performance across all demonstrations, operating continuously without internal disruption. As shown in Fig. 6, GVF-based guidance successfully enabled smooth transitions from vertiports to the corridor, with high accuracy between control commands

for both simulated and real UAVs, and consistent entry points. Some deviations were observed near entry and exit zones, primarily due to separation assurance manoeuvres. These were well mitigated, as suggested by the results in Fig. 5b. Initially, CBF served as the sole method of separation assurance under LoWC conditions; however, this led to stuck configurations when no geometrical solution was available and often slowed down corridor operations. By contrast, integrating APF allowed traffic to remain efficient by compensating with lateral deviations during LoWC events. To support this design choice, both separation assurance and collision avoidance algorithms were tested under fully simulated conditions, as described in Sec. III-B, with the comparative setups summarised in Table III. At this scale, mission efficiency was found to be highly sensitive to the LoWC threshold: CBF alone rigidly slowed traffic and could even halt operations in corridor geometries without feasible solutions. Both LoWC and NMAC thresholds were therefore adapted to the current scale and vehicle speed, with spatial detection layers proving sufficient when all UAVs shared similar performance.

From a human perception perspective, interpreting such an airspace structure proved challenging. At this scale, it was difficult to accurately judge distances and drone intent compared to straight-line flight planning. The simulator enhanced situational awareness by showing both adherence of real UAVs to the corridor and their actual separations, clarifying cases where drones appeared close but were not. Counterintuitively, BVLOS monitoring, provided accurate positioning is available, offered greater confidence in traffic supervision (when coupled with embedded drone cameras) compared to VLOS, which sometimes led to misjudgements, particularly when operators were distant from the UAVs or when UAVs were flying at higher altitudes. These observations suggest that, even if vertiport transitions within a shared corridor can be mitigated by separation assurance algorithms, entry clearance from vertiport management remains highly recommended. Such clearance would reduce the risk of unsafe situations or operator misjudgement, while also lowering stress and workload when humans are on the loop.

B. Challenges

In spite of the scalability potential of the proposed airspace design, its transition guidance, and its suitability for larger fleets of automated UAVs, several challenges and limitations were identified.

First, CBF like other geometric methods for separation assurance, perform effectively when safety thresholds are properly defined and has the advantage to be explainable. However, the LoWC and NMAC limits had to be empirically set in this work, since existing recommendations for DAA in small UAS operations are not directly applicable [22]. This raises the challenge of defining operationally valid and safe thresholds for dense corridor traffic. Second, the current 10 Hz architecture showed limitations when cruise speeds were doubled. Small overshoots in centralised monitoring or position estimation could prematurely trigger flight status changes (e.g.,

cruise or exit), leading to lag or unexpected trajectories. While safety was preserved, centralised monitoring raises critical concerns about data refresh, computation requirements, and resilience as fleet size and speed increase. Safety-critical UTM modules such as tactical conflict resolution, but not limited to, would require higher data quality and refresh rates to scale. Third, our vertiport allocation remains simplistic and was not the focus of this study. The first explored approach, based on landing-time expectations and competitive demand, offered dynamic throughput but sometimes led to unsafe separations during simultaneous take-off and landing, which had to be manually mitigated during our preliminary real demonstrations. The simplified method presented here ensures safety but requires demand to remain aligned with the number of vertiports. Lastly, simulated UAVs were modelled with simplified guidance compared to real UAVs. While this difference reduces realism, it also revealed robustness: separation was still maintained and adherence to the corridor preserved in mixed-traffic conditions.

C. Future Work & Recommendations

Several directions and on-going efforts extend this research. First, on the airspace design aspect, we are combining Reinforcement Learning with bio-inspired techniques by parameterising Slime-Mould algorithms to generate more complex circular corridors, including merging and splitting sections in dynamic environments. These environments will accommodate obstacles and no-fly zones in real time, with our GVF guidance adapting corridor's sections dynamically when the Remaining Time To Act (RTTA) allows. Second, ongoing deployment considers overlapping corridors at distinct flight levels, with clockwise and counter-clockwise flows based on shortest itineraries. Multi-lane corridors will also be investigated to assess their feasibility, their impact on separation assurance, and their ability to manage priority rules and heterogeneous traffic. Third, in a broader perspective, future efforts will integrate previous research on collision avoidance algorithms and dynamic airspace generation into the mixed-reality framework, with new simulation features. While not yet planned, contingency management requires to be set and studied in this ecosystem. Finally, larger-scale demonstrations are envisaged, potentially within U-space near Toulouse, involving denser and more heterogeneous real-traffic scenarios.

It is important to emphasise that meaningful progress in U-space research cannot be achieved without greater data sharing from the deployment of operations. A collective effort to make operational data accessible would be a catalyst for UTM development ensuring system integrity, identifying real bottlenecks, validating AI-driven approaches, and developing accurate uncertainty models.

V. CONCLUSION

This research demonstrated the operational feasibility of a dynamic shared airspace corridor for U-Space, contrasting with the conventional static reservation model. Through a mixed-reality framework integrating real and simulated drones,

we showed that GVF guidance enables smooth and predictable vertiport transitions, while a hybrid safety layer, combining CBF and APF-inspired collision avoidance, robustly maintains separation in a continuous operational scenario. The mixed-reality platform itself serves as a vital tool for safely testing and validating these future concepts. On the operational aspect, our approach opens a shift from individual UAV control to fleet management in self-organising airspace structures, potentially supporting how BVLOS operations are conducted in future U-space environments.

REFERENCES

- [1] International Civil Aviation Organization (ICAO), "Unmanned Aircraft Systems Traffic Management (UTM) – A Common Framework with Core Principles for Global Harmonization, *Edition 4*," Montreal, Canada, 2023.
- [2] J. Pons-Prats, T. Živojinović, and J. Kuljanin, "On the understanding of the current status of urban air mobility development and its future prospects: Commuting in a flying vehicle as a new paradigm," *Transportation Research Part E: Logistics and Transportation Review*, vol. 166, p. 102868, 2022.
- [3] SESAR Joint Undertaking, "Concept of Operations for European U-Space Services - Extension for Urban Air Mobility," *CORUS-XUAM, Edition 4, Horizon 2020 project, Grant agreement ID: 101017682*, 2023.
- [4] —, "EUropean Key solutions for vertiports and UAM," *EUREKA, Digital European Sky project, Grant agreement ID: 101114799*, 2023.
- [5] B. Schuchardt, T. Vu, A. Mangas, C. Nava, G. Riccardi, and M. Kolago, et al., "How to Integrate Vertiport Operations Into the Airspace? Introducing the EUREKA Project," in *AIAA SciTech 2025 Forum*.
- [6] J. Bertram and P. Wei, "An Efficient Algorithm for Self-Organized Terminal Arrival in Urban Air Mobility," in *AIAA Scitech 2020 Forum*, 2020.
- [7] M. Waltz, O. Okhrin, and M. Schultz, "Self-organized free-flight arrival for urban air mobility," *Transportation Research Part C: Emerging Technologies*, vol. 167, p. 104806, 2024.
- [8] K. Song, H. Yeo, and J. Moon, "Approach Control Concepts and Optimal Vertiport Airspace Design for Urban Air Mobility (UAM) Operation," *International Journal of Aeronautical and Space Sciences*, vol. 22, p. 982–994, 2021.
- [9] K. Song, "Optimal Vertiport Airspace and Approach Control Strategy for Urban Air Mobility (UAM)," *Sustainability*, vol. 15(1), 437, 2023.
- [10] J. Zhao, Z. Wen, K. Mohanta, S. Subasu, R. Fremond, and Y. Su, et al., "UAV Operations and Vertiport Capacity Evaluation with a Mixed-Reality Digital Twin for Future Urban Air Mobility Viability," *Drones*, vol. 9(9), 621, 2025.
- [11] Z. Ai, M. Livingston, and I. Moskowitz, "Real-time unmanned aerial vehicle 3D environment exploration in a mixed reality environment," in *International Conference on Unmanned Aircraft Systems (ICUAS)*, 2016, pp. 664–670.
- [12] European commission, "Regulation 2021/664 U-space Regulatory Framework," *Article 10, UAS flight authorisation service, April 22nd*, 2021.
- [13] Y. Tang, Y. Xu, and G. Inalhan, "Incorporating Optimisation in Strategic Conflict Resolution Service in U-space," in *11th SESAR Innovation Days*, 2021.
- [14] R. Fu, Y. Safadi, Q. Quan, and J. Haddad, "Sky Highway: An Air Traffic Structure for Low-Altitude Heterogeneous Vtol Aircraft," *Preprint, available at SSRN*, 2025.
- [15] M. Verdoucq, R. Fremond, Z. Bilgin, and M. Bronz, "Bio-inspired Algorithm for Designing an Adaptive Cyclic Corridor for UAS Traffic Management," in *IEEE/AIAA 44th Digital Avionics Systems Conference*, 2025.
- [16] R. Fremond, M. Verdoucq, Z. Bilgin, and M. Bronz, "Investigating Cyclic Airspace Corridor Optimization for UAS Traffic Management based on Deep Reinforcement Learning," in *IEEE/AIAA 44th Digital Avionics Systems Conference*, 2025.
- [17] H. de Marina, M. Bronz, and G. Hattenberger, "Guiding vector fields in Paparazzi autopilot," in *12th International Micro Air Vehicle Conference*, 2021.

- [18] A. Ames, S. Coogan, M. Egerstedt, G. Notomista, K. Sreenath, and P. Tabuada, "Control Barrier Functions: Theory and Applications," in *18th European Control Conference (ECC)*, 2019, pp. 3420–3431.
- [19] C. Reynolds, "Flocks, Herds, and Schools: A Distributed Behavioral Model," *Computer Graphics*, vol. 21, pp. 25–34, 1987.
- [20] K. Meier, A. Richards, M. Watson, G. Maalouf, C. Johnson, D. Hine, and T. Richardson, "WildBridge: Conservation Software for Animal Localisation using Commercial Drones," in *15th International Micro Air Vehicle Conference*, 2024, pp. 324–333.
- [21] ENAC Drones, "SESAR Innovation Days 2025," *Data Repository*, 2025.
- [22] EUROCAE, "Minimum Operational Performance Standard (MOPS) for Detect and Avoid (DAA) Systems," *ED-271*, 2023.